

This work was written as part of one of the author's official duties as an Employee of the United States Government and is therefore a work of the United States Government. In accordance with 17 U.S.C. 105, no copyright protection is available for such works under U.S. Law.

Public Domain Mark 1.0

<https://creativecommons.org/publicdomain/mark/1.0/>

Access to this work was provided by the University of Maryland, Baltimore County (UMBC) ScholarWorks@UMBC digital repository on the Maryland Shared Open Access (MD-SOAR) platform.

Please provide feedback

Please support the ScholarWorks@UMBC repository by emailing scholarworks-group@umbc.edu and telling us what having access to this work means to you and why it's important to you. Thank you.

Characterization of the Reflectance Anisotropy of Three Boreal Forest Canopies in Spring–Summer

Donald W. Deering,^{*} Thomas F. Eck,[†] and Babu Banerjee[†]

As a part of the Boreal Ecosystem–Atmosphere Study (BOREAS), measurements of the spectral reflectance anisotropy of three boreal forest canopies were studied for cloudless sky conditions at the phenological growth stages which were at or near maximum leaf area index at each site. The three sites were relatively homogeneous mature stands of black spruce, jack pine, and aspen located in the southern boreal zone of central Saskatchewan. Measurements of the spectral bidirectional reflectance factors with a 15° instrument field of view in three spectral bands centered at 662 nm, 826 nm, and 1658 nm were made with the PARABOLA instrument over a range of solar zenith angles typically varying from 35° (near solar noon) to 70°. The measured reflectance factors showed large anisotropy at all three sites and for all three wavelengths, with prominent backscatter peak reflectances, and strong retro solar view angle (hot spot) maximum reflectances in the visible (662 nm) and shortwave infrared (1658 nm) for the jack pine and black spruce sites, with a less pronounced hot spot at the aspen site. Pronounced effects of canopy and understory shadowing in the visible, as a function of solar zenith angle (SZA), were observed for the black spruce and jack pine sites, with resultant large linear increases in computed normalized difference and simple ratio vegetation indices as SZA increased for near-nadir view angles. Hemispheric spectral reflectances or spectral albedos were computed from angular integration of PARABOLA measured bidirectional reflectances. Visible (662 nm) hemispheric reflectances for the jack pine and black spruce canopies showed very little variation with solar zenith angle, while

near-infrared hemispheric reflectances increased strongly with increasing SZA. Estimates were made of the total shortwave albedo for the aspen and jack pine sites from irradiance and reflectance weighting of the spectral hemispheric reflectances in the three measured wavelengths. Comparison of estimated to pyranometer measured total albedo showed all estimates to be biased high, but only by about 0.007–0.018, depending on which of two sets of pyranometer measured albedos were utilized for the comparison. The measured bidirectional reflectance factor (BRF) data sets reported in this study coupled with ancillary data of biophysical parameters collected at the same sites by BOREAS researchers provide a unique data set for the development and characterization of canopy bidirectional reflectance modeling and for the interpretation of remotely sensed data for boreal forest canopies. ©Elsevier Science Inc., 1999

INTRODUCTION

Boreal forests play an important role in the exchange of CO₂ between the biosphere and atmosphere, due to their large biomass, primary productivity, and extensive circumpolar areal coverage. The studies of D'Arrigo et al. (1987) suggest that the seasonal growth of boreal forests (approximately 50–70° N latitude) account for approximately 50% of the mean seasonal CO₂ amplitude measured at Pt. Barrow, Alaska and approximately 30% of the CO₂ signal at Mauna Loa, Hawaii, which is a more globally representative site. Modeling of the global climatic response to increasing atmospheric CO₂ concentrations has in many simulations (Schlesinger and Mitchell, 1987) shown that the largest increases in temperature globally will occur in the latitude range 45–65° N, which coincides closely with the boreal forest region. Some of these

^{*} NASA/GSFC, Biospheric Sciences, Greenbelt

[†] Raytheon STX Corporation, NASA/GSFC, Greenbelt

Address correspondence to Thomas F. Eck, Code 923, NASA/GSFC, Greenbelt, MD 20771. E-mail: teck@ltpmail.gsfc.nasa.gov

Received 26 January 1998; revised 18 August 1998.

simulations also find a significant drying of soil moisture at mid to high latitudes during the summer months.

The forest landscape spatial and temporal variability in ecosystems and species within a boreal forest region results from many factors such as fire history and past fire succession, soil variations (including soil moisture, temperature, nutrients, and permafrost), and topographic effects (slope, aspect, and elevation) (Bonan, 1991a). These and several climatic factors (principally temperature and precipitation) are the primary controlling factors in the landscape variability in the circumpolar boreal forests. Potential warming and drying of the boreal zone as simulated for increasing atmospheric CO₂ concentrations may affect directly or indirectly many of these factors, such as possible increases in fire frequency. Jacoby and D'Arrigo (1995) have shown from tree ring analysis that annual temperatures in the boreal forest region of Alaska have increased 2–3°C over the past century, an increase which is also evident in recorded temperature. Their study suggests that the recently increased temperature coupled with drier conditions may be resulting in moisture stress limiting tree growth and also to conditions favorable to an increase in tree damaging insects.

Satellite platforms with remote sensing instruments provide the most powerful technique available for the monitoring of the circumpolar boreal forest conditions over large regions at a sufficient temporal and spatial resolution. The ability to monitor the state and changes of state of the boreal forest globally may be very valuable in the detection of biospheric responses to global change. One use of the application of satellite data to large area analysis of the boreal forest was shown by Bonan (1991b), who found that the normalized difference vegetation index (NDVI) derived from the AVHRR sensor on a NOAA satellite, accounted for 85% of the annual tree carbon flux averaged over the landscape. However, he noted problems in the interpretation of the NDVI data such as background reflectance effects (especially snow) and solar angle effects. Bonan (1993) also pointed out the importance in discriminating between needleleaf coniferous and broadleaf deciduous forest types within the boreal zone when estimating photosynthesis and in the determination of leaf area index for all species. Satellite algorithms are currently available and others being developed to retrieve estimates of these parameters from remote sensing of bidirectionally reflected radiances (e.g., Chen and Cihlar, 1996; Spanner et al., 1990).

In order to more fully exploit the potential of satellite-based remote sensing of forest canopy parameters, such as the use of vegetation indices and retrieval of leaf area index and albedo values, further development of physical vegetation reflectance models is needed. Verstraete et al. (1996) have pointed out that more effort should go into the validation of these models, but that a major obstacle to validation "is the lack of simultaneous remote sensing, field, and laboratory acquisitions" (p. 208),

along with the collection of data describing associated ancillary parameters. They further state: "The spectral exploitation of the data cannot be done without taking the directional aspects into account. The lack of directional sampling in current data sets poses significant problems in the proper treatment of this issue (p. 212)."

Due to logistical difficulties in acquiring field measurements of the bidirectional reflectance of forest canopies, there have been very few measurements, some of which have been restricted to only a very small range of solar zenith angles. Kleman (1987) and Kimes et al. (1986) utilized helicopter-based instrumentation to measure forest canopy bidirectional reflectance. Kriebel (1978) and Ranson et al. (1994) utilized airplane-mounted instruments to obtain bidirectional reflectance measurements of forest canopies, and Deering et al. (1994) took measurements of a spruce-hemlock canopy from the near surface platforms of a tower and a pneumatic telescopic mast.

In this article we present measurements of forest canopy bidirectional reflectance factors for three boreal forest species: black spruce (*Picea mariana*), jack pine (*Pinus Banksiana*), and trembling aspen (*Populus tremuloides*). These three species are the dominant ones in the boreal forest region of central Saskatchewan, and the three sites are near the southern limit of the boreal zone in this region. These data were taken as a part of the international Boreal Ecosystem Atmosphere Study (BOREAS; Sellers et al., 1995) during which many researchers participated in data collection of a wide range of observations of ecological and atmospheric parameters at these same sites. Therefore, there is a wealth of ancillary measurements which complement the bidirectional reflectance measurements we report here, for the purposes of validation of forest canopy bidirectional reflectance models, and the associated retrieval of forest canopy parameters from remote sensing measurements.

INSTRUMENTATION AND METHODS

The bidirectional reflectance factor (BRF) measurements were made with the PARABOLA instrument on the three selected boreal forest study sites. The PARABOLA instrument (Deering and Leone, 1986) is a two-axis scanning head, three-channel (red, near-infrared, and short-wave infrared: 650–670 nm, 810–840 nm, and 1620–1690 nm, respectively), motor-driven radiometer that permits acquisition of radiance data for almost the complete (4 π) sky- and ground-looking hemispheres in 15° instantaneous field of view (IFOV) sectors in 11 s. A downward viewing 35 mm camera with a 16 mm lens was used to document the forest canopy for every PARABOLA data acquisition.

In order to spatially sample the forest canopy BRF at the sites we studied in the BOREAS experiment, the PARABOLA instrument was suspended from a tram



Figure 1. Photograph of steel cables-tram system supported between two towers, with the PARABOLA instrument mounted on the tram, at the aspen site in Prince Albert National Park, Saskatchewan.

which traversed a pair of fixed steel cables between two towers (Fig. 1). One of the towers was a scaffold type with staircase and platforms from which we operated the instrument control panel and the other tower was a triangular truss (0.3 m) aluminum Rohn tower located 70 m to the north (approximately) of the scaffold tower. The towers ranged in height from approximately 24 m to 38 m, and the resulting tram cable height was about 13–14 m above the canopy height at each site. This sampling height and instrument IFOV of 15° resulted in a nadir view footprint size at canopy top level of $\sim 9 \text{ m}^2$, increasing to $\sim 79 \text{ m}^2$ at 60° off-nadir view angle. The tram was slid along the steel cables by a set of nylon ropes, held near the cables by a set of steel rings, and the tram position was varied by pulling the ropes either from the scaffold tower or by means of a pulley from the ground below the Rohn tower.

The sampling strategy we employed, in order to attempt to adequately sample the spatial variance of the forest canopies, was to take PARABOLA instrument data scans with the instrument located at distances from 25 m to 5 m from the scaffold tower, at 2 m increments. This resulted in a total of 11 subsites being sampled along the tram at each solar zenith angle (SZA). The sequence of measurements at 11 subsites took approximately 10–20 min resulting in a change of solar zenith angle of about $\pm 2^\circ$ from the mean at 70° SZA to approximately $\pm 0.3^\circ$ from the mean at 35° SZA. Clouds permitting, the sampling was repeated at 5° SZA increments from 75° or 70° to the SZA near the minimum (solar noon) value.

In order to characterize the spatially averaged canopy bidirectional reflectance factors, we have computed average reflected radiances from binning of all the observations which fall into equal increment view azimuth and view zenith angle bins. The bins are defined in 15° angular increments in view zenith angle and 30° angular increments of view azimuth angle with one of the bins being centered on the solar principal plane. We define the solar principal plane as the 0 – 180° azimuth transect with 0° as the azimuth of the Sun and 180° as opposite the solar position. Before inclusion in a view zenith-azimuth bin, the observations are screened automatically by the processing software if the instrument is viewing the tower, tram support structures, or tower shadows (calculated from known and fixed locations of objects and solar angle geometries). Therefore, given that we have the premeasured angular relationships between instrument view zenith angles and obstruction of the instrument field of view by noncanopy structures such as the tram and towers, these observations are removed before binning. Data are also automatically screened prior to binning for electronic noise which results in sensor saturation. After binning, the data are checked for very low values of NDVI $[(\text{Near-Infrared} - \text{Visible})/(\text{Near Infrared} + \text{Visible})]$, which may result from viewing other non-

canopy structures present at the site (such as other shorter scaffold towers used for canopy sampling). Once all data screening checks are completed, the mean and standard deviation of the radiances in the three PARABOLA channels are computed. For cases where all the observations falling within a bin are screened, then the value from the “mirror” or opposite side of the solar principal plane is used in that bin, thus assuming symmetry about the solar principal plane. If the mirror side value is not available, then the value for that bin is interpolated from adjacent bins. Only a small percentage of bins have all observations screened from them due to data quality checks.

In addition to the PARABOLA instrument, a downward viewing Eppley PSP pyranometer (0.28 – $2.8 \mu\text{m}$) and downward viewing Skye-Probetech SE-510 (0.4 – $0.7 \mu\text{m}$) sensor were also affixed to the aluminum tram frame. These instruments in conjunction with two upward viewing instruments of the same types, mounted on top of the scaffold tower, enabled us to compute both broadband “total” (0.28 – $2.8 \mu\text{m}$) albedo and Photosynthetically Active Radiation (PAR, 0.4 – $0.7 \mu\text{m}$) albedo over the sites.

Characterization of spectral solar irradiance was carried out using two separate techniques. First, a Barnes Modular Multiband Radiometer (MMR) was mounted above a barium sulfate (BaSO_4) reference panel, both clamped to the tower above the canopy top in order to sample the spectral downwelling irradiance. The MMR and PARABOLA were intercalibrated at the GSFC 1.8 m integrating sphere radiance source. The MMR measurements of the BaSO_4 were corrected for panel reflectance anisotropy which had been previously characterized using the procedure of Jackson et al. (1987). However, due to different bandpasses of the PARABOLA and MMR instruments (e.g., PARABOLA 810 – 840 nm versus MMR 750 – 880 nm), the MMR response to different total columnar atmospheric water vapor amount differed from the PARABOLA due to different water vapor transmittances. Therefore, we utilized the cloudless sky spectral irradiance model which is an integral part of the 6S model (Vermote et al., 1997) using measured aerosol optical depths, total water vapor, and aerosol volume size distributions from Cimel automatic spectral Sun and sky scanning radiometers located in the southern BOREAS study area (Markham et al., 1997). The aerosol volume size distributions retrieved from the Cimel Sun-sky scanning radiometer (Nakajima et al., 1996) are utilized in the 6S model to compute the aerosol scattering phase function from Mie theory, given assumed values of the refractive index. For our analysis, we assumed the aerosol single scattering albedo to be 0.95, which is representative of remote background aerosol (Waggoner et al., 1981). However, for low AOT conditions under which our measurements were taken (see Table 1), variations in single scattering albedo have little influence on irradi-

Table 1. Aerosol Optical Thickness (AOT) and Precipitable Water (PW) Measured by Automatic Sunphotometers in the BOREAS Southern Study Area for the Dates of the PARABOLA Measurements Presented

Date	AOT (670)	AOT (870)	AOT (1020)	PW (cm)
31 May 1994	0.057	0.048	0.045	1.1
7 June 1994	0.041	0.036	0.034	0.6
21 July 1994	0.045	0.037	0.037	2.3

ance. The total ozone amount utilized in the 6S model calculations were climatological means from London et al. (1976). It is noted that the PARABOLA instrument does not measure direct solar irradiance, since the detector saturates when viewing the Sun. With the low aerosol optical depth conditions under which the measurements described here were taken (Table 1), the diffuse fraction of total spectral irradiance is relatively small, and under these conditions direct plus diffuse solar irradiance may be accurately modeled using the measured aerosol optical depth data as the principal parameter.

For PARABOLA Channel 1 (650–670 nm; with no water vapor absorption) the 6S computed and MMR measured irradiances agreed very well, typically within 1–3%. However for PARABOLA Channel 2 (810–840 nm), the differences between the two techniques varied from approximately 1% to 15% dependent on water vapor amount and solar zenith angle. Differences between the two techniques for PARABOLA Channel 3 (1620–1690 nm) were intermediate to those found for the other channels, since the water vapor transmittance differences for the two instrument bandpasses were less in Channel 3 than for Channel 2. Therefore, due to the differing effects of the water vapor transmittances for the differing bandpasses of the two instruments, we utilized the spectral irradiance computed from 6S in our calculations of reflectance factors presented in this article. These irradiance values were used to compute reflectance factors (RF) in each of the three PARABOLA wavelengths, given in Eq. (1) as

$$RF = (\pi \circ R) / I, \quad (1)$$

where R is the spectral reflected radiance, and I is the spectral solar irradiance.

Table 1 gives the values of aerosol optical depth and precipitable water measured by the Cimel radiometers at three wavelengths for the days of the PARABOLA measurements that we present in this article. The aerosol optical depths are stable and low on these days, which is representative of conditions in the region when forest fire smoke is not present.

SITE DESCRIPTIONS

The measurements we report in this article were made at three boreal forest sites in central Saskatchewan, Canada in 1994. These sites are located in the Southern

Study Area (SSA) of the BOREAS experiment, and are near to the southern boundary of the boreal forest ecosystem in that region. The BOREAS designated names for these sites are SSA Old Black Spruce (53.99° N, 105.12° W), SSA Old Aspen (53.63° N, 106.20° W), and SSA Old Jack Pine (53.916° N, 104.69° W). In this article the sites will simply be referred to as black spruce, jack pine, and aspen.

At the black spruce site, tree cover was primarily made up of black spruce (height: 0–10 m), with scattered emergent tamarack (10–16 m). The black spruce trees age ranged up to 155 years, and the total stem density (of all species) at the site was 8040 live stems/ha, with a basal area of 40 m²/ha. Young black spruce make up the understory, and the ground cover is composed of sphagnum moss with feather moss, bog cranberry, and labrador tea. Canopy closure averaged about 55%, and the soil drainage ranged from imperfect to poor (Sellers et al., 1994). The leaf area index (LAI) measured by optical methods, using an LAI-2000 at this site in spring 1994 was 3.7 (Chen et al., 1997a). This LAI estimate does not include the ground cover (moss). This compares to a midsummer 1994 value of LAI of 4.0 at the black spruce site (Chen et al., 1997a). Photographs of the black spruce site, showing above canopy, below canopy, and ground cover are presented in Figure 2. It is noted that, although analysis of the photos was beyond the scope of this study, quantitative classification into sunlit/shadowed and crown/understory of these images could provide additional information for modeling studies of these sites.

The aspen site was located near the southern part of Prince Albert National Park and contains mostly mature trembling aspen in the primary stratum (with a few balsam poplar), at an average height of 21 m and average age of 60 years. The stem density of this site totaled 1244 live stems/ha, with a basal area of 38 m²/ha. A dense growth of hazelnut shrubs (2–3 m height) with some wildrose comprised the understory, and the groundcover was approximately 50% leaf litter with various grasses and herbs. The estimated canopy closure, including hazelnut understory, averaged 89%, and the soil was described as ranging from well drained to poor (Sellers et al., 1994). The estimated LAI at this site for 21 July 1994 (the date of measurements presented in this article) was 2.30 for the aspen and 3.23 for the hazelnut (site total LAI of 5.53), also determined optically with an LAI-2000 instrument (Chen et al., 1997b). Photos taken at



a



b



c

Figure 2. Photographs of the black spruce site a) above the canopy—oblique view, b) below the canopy—oblique view, and c) nadir view of the lower canopy/ground cover. Note the mixture of emergent tamarack trees among the spruce (a) and mixture of mosses, shrubs, and saplings in the understory (c).



a



b



c

Figure 3. Same as Figure 2 but for the aspen site. Note the high visible reflectance of the aspen trunks (b) and the dense, high LAI, hazelnut shrub understory (c).

the aspen site showing the above and below canopy structure are shown in Figure 3.

The jack pine site was a pure stand with approximate age of 60–75 years. The tree height ranged from 11 m to 14 m, and the total stem density was 2700 live stems/ha with a basal area of 58 m²/ha. The understory was composed of scattered clusters of green alder, and the ground cover consisted of bearberry, feather moss, and lichens. The predominant ground cover, in areal coverage and in influence on reflectance for the area sampled by the PARABOLA, was a lichen called reindeer moss (*Cladonia*), which is light in color. Canopy closure was estimated to be approximately 61%, and the soil was sandy and well drained (Sellers et al., 1994). The estimated canopy LAI for this jack pine site in late spring 1994 was 2.2 (Chen et al., 1997a), which does not include an estimate of the ground cover LAI contribution, which is quite small for this site. This compares to a mid summer 1994 value of LAI of 2.6 at the jack pine site (Chen et al., 1997a). Figure 4 presents photographs of the above and below canopy structure of this site.

RESULTS AND DISCUSSION

Spectral Bidirectional Reflectance Factors

An overall view of the bidirectional reflectance of the three boreal forest sites studied is shown in three-dimensional graphic presentation in Figure 5. These graphs show the comparison of the spectral bidirectional reflectance factors for the jack pine, black spruce, and aspen at 45° SZA. All three forest types show some similarities in the pronounced increase in bidirectional reflectance in the backscatter direction, peaking at the retro-solar angle (45° backscatter view angle). This local maximum peak at the retro solar view angle is particularly strong in the visible (662 nm) wavelength and much less pronounced in the near-infrared wavelengths, as will be discussed below. All three forest canopies show elevated reflectances in the solar principal plane except in the forwardscatter view direction. Forwardscatter direction reflectances are relatively low and constant, especially for the jack pine and black spruce sites, with the aspen site showing some increase as view zenith angle increases.

The dynamics of the spectral bidirectional reflectance factors in the solar principal plane, for SZA ranging from about 70° to 35°, for the three boreal forest canopies studied are shown in Figure 6. The dates of these measurements from 31 May 1994 (for jack pine) to 21 July 1994 (for aspen) represent times of phenological development, which are near to peak leaf area for these sites. These dates were also chosen for conditions of low aerosol loading which are typical for this region when not being affected by forest fire smoke. Measurements in the solar principal plane are shown at 15° angular increments in view angle, since the angular instantaneous FOV of the

PARABOLA is 15°, from 75° off-nadir view angle in the backscatter direction to –75° off-nadir view angle in the forwardscatter direction.

Nadir Reflectances

For the nadir view angle direction, (Fig. 7) the red (662 nm) reflectance factors for both of the coniferous sites (black spruce and jack pine) show a nearly linear decrease as solar zenith angle increases due to the viewing of more dark shadows for these canopies with incomplete coverage. Similar shadowing effects at visible wavelengths at nadir view have been observed for shinnery oak (shrub sized trees in sandy soil) by Deering et al. (1992) and for balsam fir trees arranged on a white background by Ranson et al. (1986). However, for the deciduous aspen canopy, the nadir red reflectances are nearly constant as a function of SZA due to the lack of strong differences in reflectance between the sunlit and shadowed understory hazelnut canopy which is highly absorbing at this wavelength due to the high LAI. These differences in visible shadow effects at these sites are evident in the downward viewing hemispherical photographs for the sites (Fig. 8) at the SZAs of 40° and 65°. In the near-infrared (near-IR, 826 nm) waveband, however, the only site showing a decrease in reflectance as SZA increases is the black spruce, as a result of the very dense upper canopy architecture, which results in absorption even in the near-IR, which has high leaf transmittance and reflectance, resulting in multiple scattering and filling of shadows at the other two sites. The jack pine site shows a nearly constant near-IR nadir reflectance as a function of SZA, while the aspen site exhibits a trend of increasing nadir reflectance as SZA increases. At the shortwave infrared waveband (SWIR), 1658 nm, the trends in nadir reflectance are similar to those seen for visible wavebands for all three sites. This is a result of shadowing in the SWIR due to absorption by leaf water content (Hunt and Rock, 1989) rather than by chlorophyll absorption in the visible spectrum. Therefore, the fairly constant SWIR nadir reflectance as a function of SZA at the aspen site may be due in part to the high absorption at low SZA by the high LAI hazelnut understory canopy, thus resulting in little change in reflectance from shadowing at higher SZA.

Hot Spot Reflectances

A local maximum in bidirectional reflectance factors in the solar principal plane at the retro-solar view angle is noted for all three forest canopy sites (Fig. 6), especially in the red (662 nm) waveband. This peak reflectance region in the backscatter view direction is often referred to as the hot spot. Hapke et al. (1996) have shown, from measurements of the bidirectional reflectance in circularly polarized light, that, for vegetation canopies where the size of the scatterers are large relative to the wave-



a



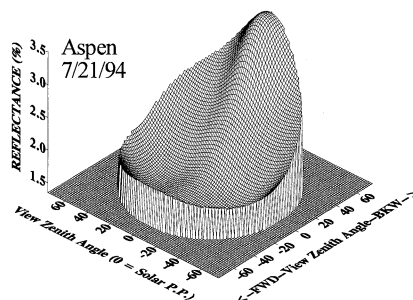
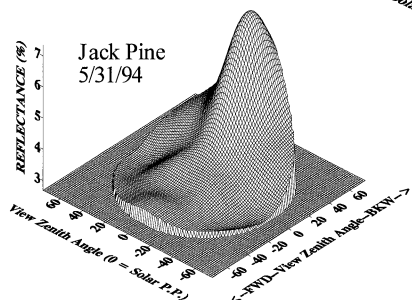
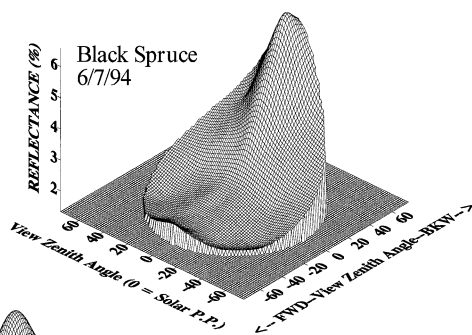
b



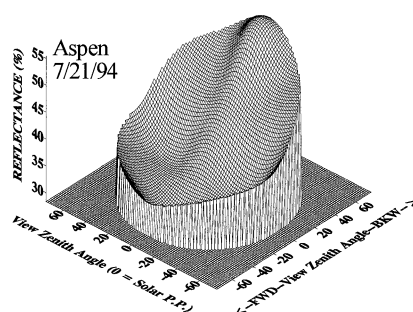
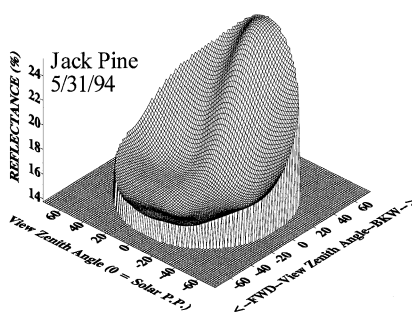
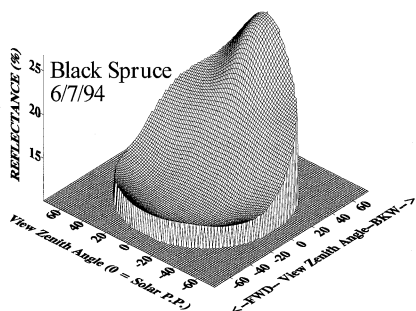
c

Figure 4. Same as Figure 2 but for the jack pine site. Note the relatively open canopy structure (a) and the mixture of light colored reindeer moss and leaf litter (needles) in the ground cover (c).

662 nm



826 nm



1658 nm

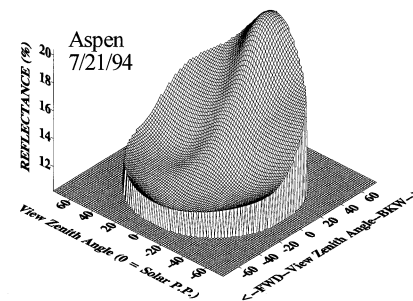
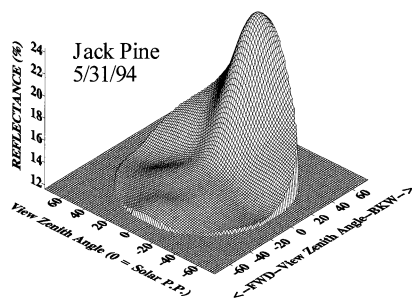
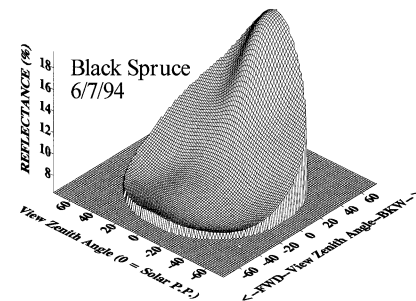


Figure 5. Three-dimensional (3-D) graphs of the bidirectional reflectances at each of the three sites at 45° SZA. Data for the three PARABOLA instrument wavebands with center wavelengths of 662 nm, 826 nm, and 1658 nm are shown.

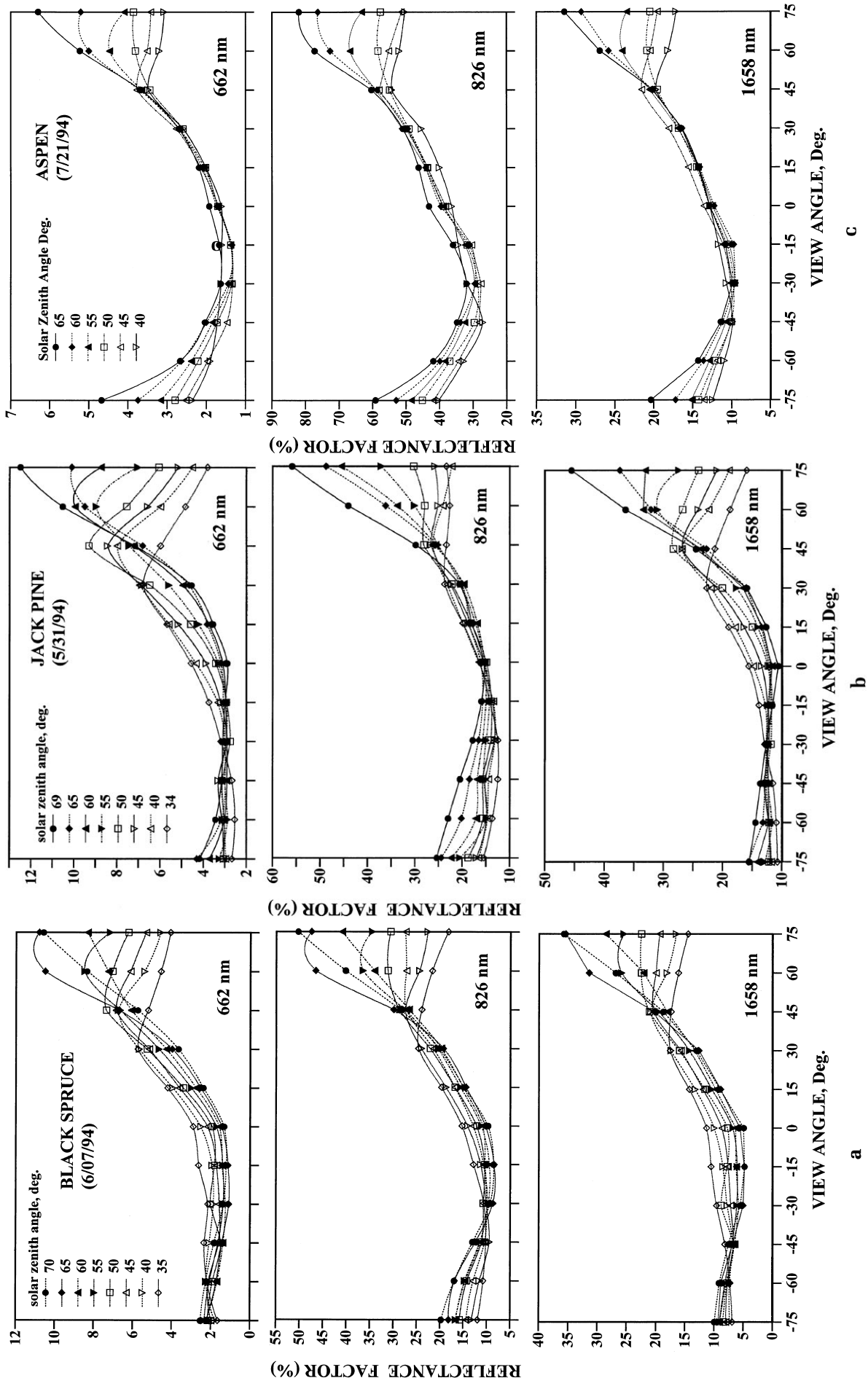


Figure 6. Spectral reflectance factors in the solar principal plane for a) black spruce, b) jack pine, and c) aspen, for the solar zenith angle range of approximately 35–70°.

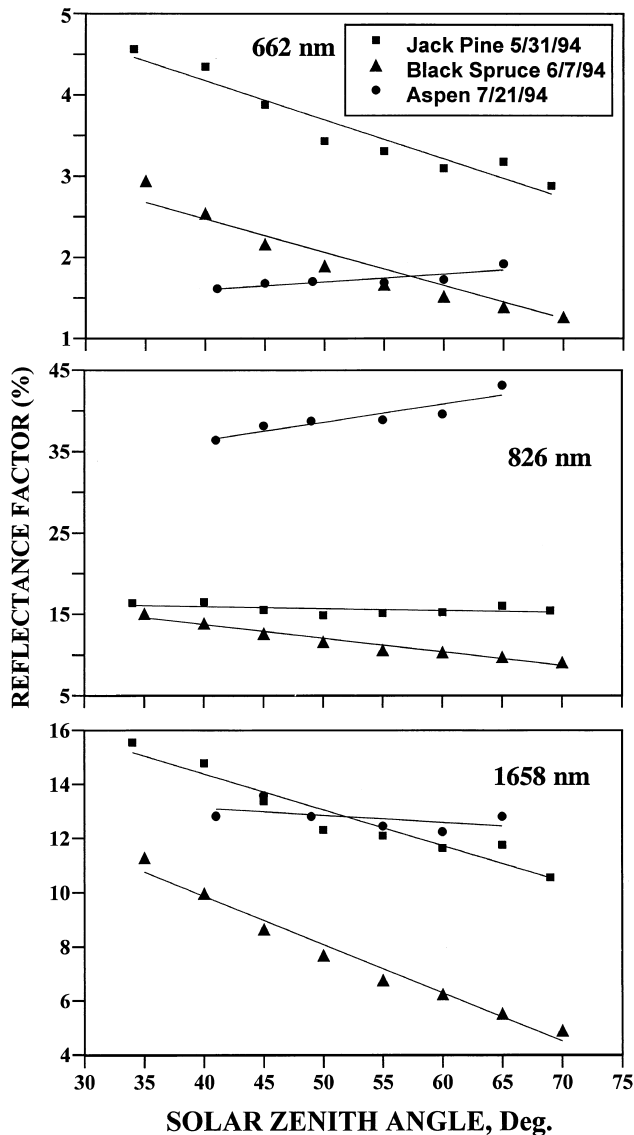


Figure 7. Spectral reflectance factors in the nadir view direction, as a function of solar zenith angle, for all three sites.

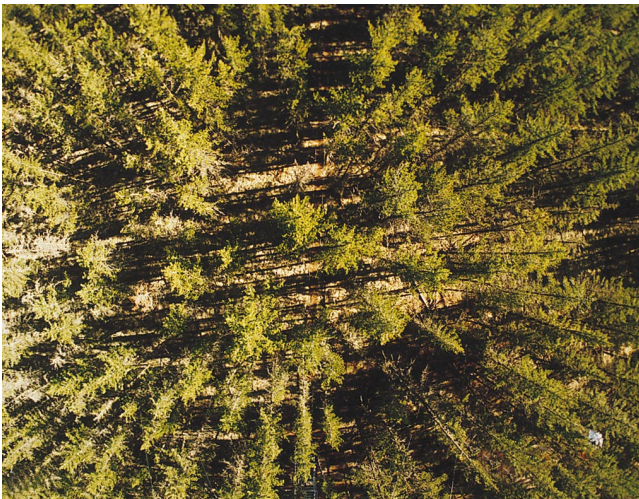
length of the incident radiation, the primary mechanism for the hot spot peak is shadow hiding. This results from each scatterer hiding its own shadow when viewed from the retro-solar direction. Their measurements included samples of spruce needles and for these needles it was determined that the hot spot was caused by shadow hiding. However, Hapke et al. (1996) found that the hot spot for moss, which contains scatterers that are similar to wavelength size, is caused largely by coherent backscatter. Therefore, for these three boreal forest sites, it is most likely that shadow hiding is the dominant physical mechanism responsible for the hot-spot effect; however, there may be some contribution of coherent backscatter at the black spruce and jack pine sites from mosses growing both epiphytically on the branches of the trees and also on the forest floor. There is very little moss present at the aspen site.

The much more prominent hot spot, in the red (662 nm) waveband, for the jack pine and black spruce sites, compared with the aspen site is due in part to the higher contrast in the background and understory reflectance elements to upper canopy elements at these sites. This is particularly noticeable for the jack pine site, which has a dominant layer of reindeer moss, which is bright in the visible wavelengths. At the aspen site the shadowed and sunlit understory reflectances are both low due to the high LAI and strong chlorophyll absorption at 662 nm. Also, the upper tree crown architecture is more open in the aspen site compared to more densely formed tree crowns at the jack pine and especially the black spruce, which result in denser shadowing. The much lower magnitude of the hot spot relative maximum in the near-infrared wavelength (826 nm) at the black spruce and jack pine sites can be attributed partly to the high level of multiple scattering and higher leaf transmittance at this wavelength, thus resulting in filling in of shadows. The hot spot characteristics in the shortwave infrared waveband for the two coniferous sites is somewhat like the visible waveband due to the absorption by liquid leaf water in this wavelength region, resulting in shadowing effects.

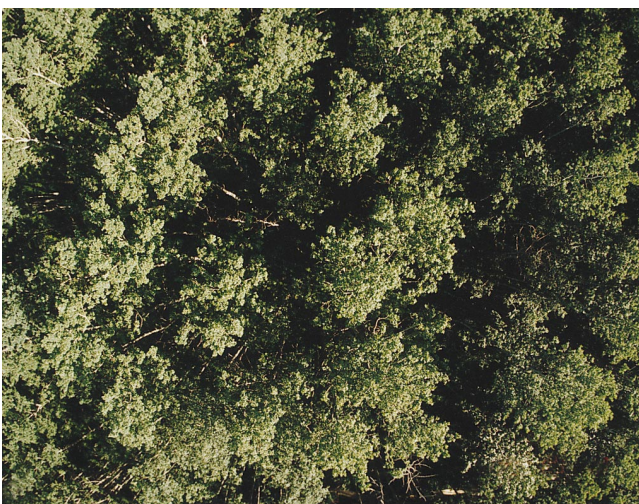
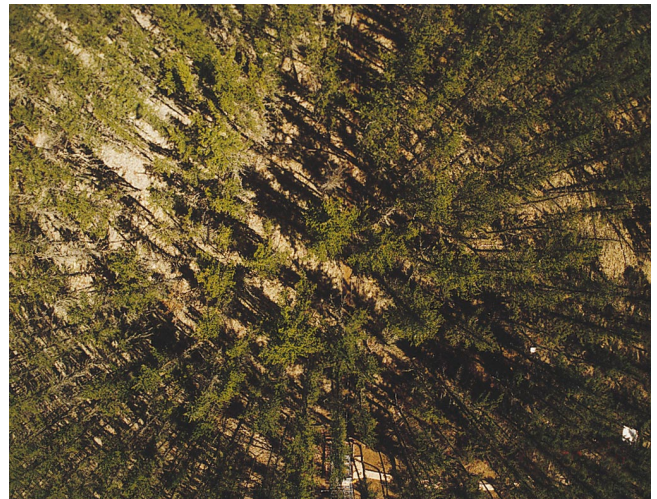
Hot spot reflectances can have a narrow angular width with sharp and high peak values. Since the angular FOV of the PARABOLA instrument is 15° , the full angular structure and peak reflectance of the hot spot tends to be smoothed due to averaging over the wide FOV of this instrument. Jupp and Strahler (1991) have shown through physical modeling of vegetation canopy radiative transfer that the angular width of the hot spot is related to the ratio of leaf diameter to canopy depth, with the angular hot spot widening as leaf diameter increases relative to canopy depth. They note that, for tree canopies, crown size rather than leaf size is important in scaling of the hot spot effect. There are very few reported measurements of the hot spot in the literature; however, Kusk (1991) made narrow FOV (1°) measurements of clover and barley canopies. He found distinct hot spot maxima in the red waveband, although the angular widths of the hot spot region for these canopies were not very narrow, approximately $20\text{--}25^\circ$. However, the gradient in reflectance in the hot spot region was sharp with a distinct peak which would have been smoothed out if measured with a 15° FOV, such as the PARABOLA instrument FOV. Breon et al. (1997) present measurements from the POLDER instrument (mounted on a helicopter) of the solar principal plane BRDF of the same BOREAS black spruce site and the same date of acquisition as our measurements. The nadir reflectances at 660–670 nm are very similar, with PARABOLA values about 2.5% while POLDER is about 2.0%. However, the PARABOLA measured hot spot peak reflectance is about 6% at 35° solar zenith angle, while it is about 8% from POLDER at 34° . This direct comparison of 15° FOV



a



b



c



Figure 8. Downward viewing wide angle photographs showing first, 65° SZA, and second, 40° SZA, illumination for a) the black spruce, b) the jack pine, and c) the aspen sites. Note that these photos show the area below one of 11 subsites sampled along the tram-cable system.

PARABOLA measurements with high angular resolution (less than 0.4°) POLDER data quantifies the effect of the smoothing of the hot spot reflectance maximum by the PARABOLA. Therefore, all of our measurements presented in this article do not portray the actual shape and peak value of the hot spot reflectances, but they do accurately represent the hot spot effects averaged over 15° and thus give valuable information regarding changes in hot spot reflectances with solar zenith angle and in differences in angular averaged hot spot magnitude between sites.

Forward Scatter Reflectance in the Solar Principal Plane

The forward scatter reflectances from -30° to -75° (Fig. 6) show much less dynamics than the backscatter hot spot reflectances do, both as a function of solar zenith angle and view zenith angle. The two coniferous canopies show relatively constant reflectance as a function of view angle and SZA when viewing the shadowed sides of the canopy. However, there is a slight measured increase in reflectance for these two canopies at large SZA, as view angle increases due to transmittance and specular reflectance effects. This increase is especially evident in the near-infrared waveband, where leaf transmittance and multiple scattering are much greater than in the visible waveband. The deciduous aspen canopy on the other hand, shows pronounced increases in reflectance at the large view angles of 60° and 75° forwardscatter due to the higher canopy transmittance and perhaps specular reflectance resulting partly from the less clustered leaf architecture and different leaf shape and angular distribution of this species.

Reflectance Variation as a Function of View Azimuth

The reflectances for four azimuthal plane transects at 30° azimuth angle increments, for SZA of 45° , are shown in Figures 9a–c. For all three sites there is a conspicuous absence of hot-spot peak reflectivity for the 30 – 210° azimuth transect which is only 30° in azimuth from the solar principal plane, thus confirming that the hot spot is a relatively narrow feature in the azimuth plane also. Jupp and Strahler (1991) also modeled the same type of reduction in hot spot effect when viewing at azimuth angles off the solar principal plane. Therefore, in order to utilize the hot spot signature in remote sensing applications it is necessary to make measurements very close in azimuth angle to the solar principal plane.

For the plane perpendicular to the principal plane, the reflectances for the black spruce site were relatively constant as a function of view angle. Symmetry is assumed for the plane perpendicular to the solar principal plane so the data from the least contaminated side of the solar principal plane is used in our analysis. The jack

pine site also shows relatively small reflectance change in the plane perpendicular to the solar principal plane with the exception of an increase in the NIR at 60° and 75° view angle. However, for the aspen site, which has two-layer canopy structure with higher LAI in the understory, there is first a decrease in reflectance when viewing away from nadir and then an increase at large off-nadir view angles. This is particularly pronounced at the NIR waveband, and may be due to viewing a higher percentage of the sides of tree boles and bark when viewing at moderate off-nadir angles, 15 – 45° , and then viewing only the aspen crowns at large view angles, 60 – 75° (see Fig. 3).

Reflectance Magnitude Comparison

A comparison of the reflectance magnitudes for the three sites in the solar principal plane, at 45° SZA, is shown in Figure 10. The difference in hot spot peak magnitude in the red waveband is large, with the aspen site having a much lower value (as discussed previously), although nadir red reflectances of the aspen and spruce are very similar. The higher values of red reflectance for the jack pine site is due in part to the influence of light colored reindeer moss (which has little chlorophyll) at this site.

For the NIR waveband, both the jack pine and black spruce exhibit similar reflectance magnitudes, while the reflectances of the aspen are nearly twice as high at all view angles in the solar principal plane. The much higher NIR reflectances for the aspen site can be attributed to a combination of the following factors: higher total LAI of the aspen site (5.5 versus 2.2 for jack pine and 3.7 for black spruce), canopy geometry including shoot geometry (coniferous species exhibit dense clustering of needles, thus giving higher penetration of radiation into the canopy than broadleaf species for the same LAI), understory reflectance differences and leaf reflectance differences (both of which exhibit higher NIR reflectance for the aspen site).

For the shortwave infrared waveband, the jack pine shows the highest reflectance values while the black spruce exhibits the lowest. Since the SWIR reflectance decreases with increased leaf water content (Hunt and Rock, 1989), the moist conditions of the black spruce site, which was boggy with sphagnum moss and some standing water in spring 1994, explains the low SWIR reflectance for this site. The jack pine site on the other hand has very well-drained sandy soil, and therefore of the three sites studied it has the least soil moisture.

A comparison between the reflectance factors of the BOREAS jack pine and black spruce sites and a spruce-hemlock site in Maine (Deering et al., 1994) and a spruce site in Sweden (Kleman, 1987) is shown in Figure 11. The data are shown for a nominal solar zenith angle of approximately 50° (range: 49 – 54°) in the solar princi-

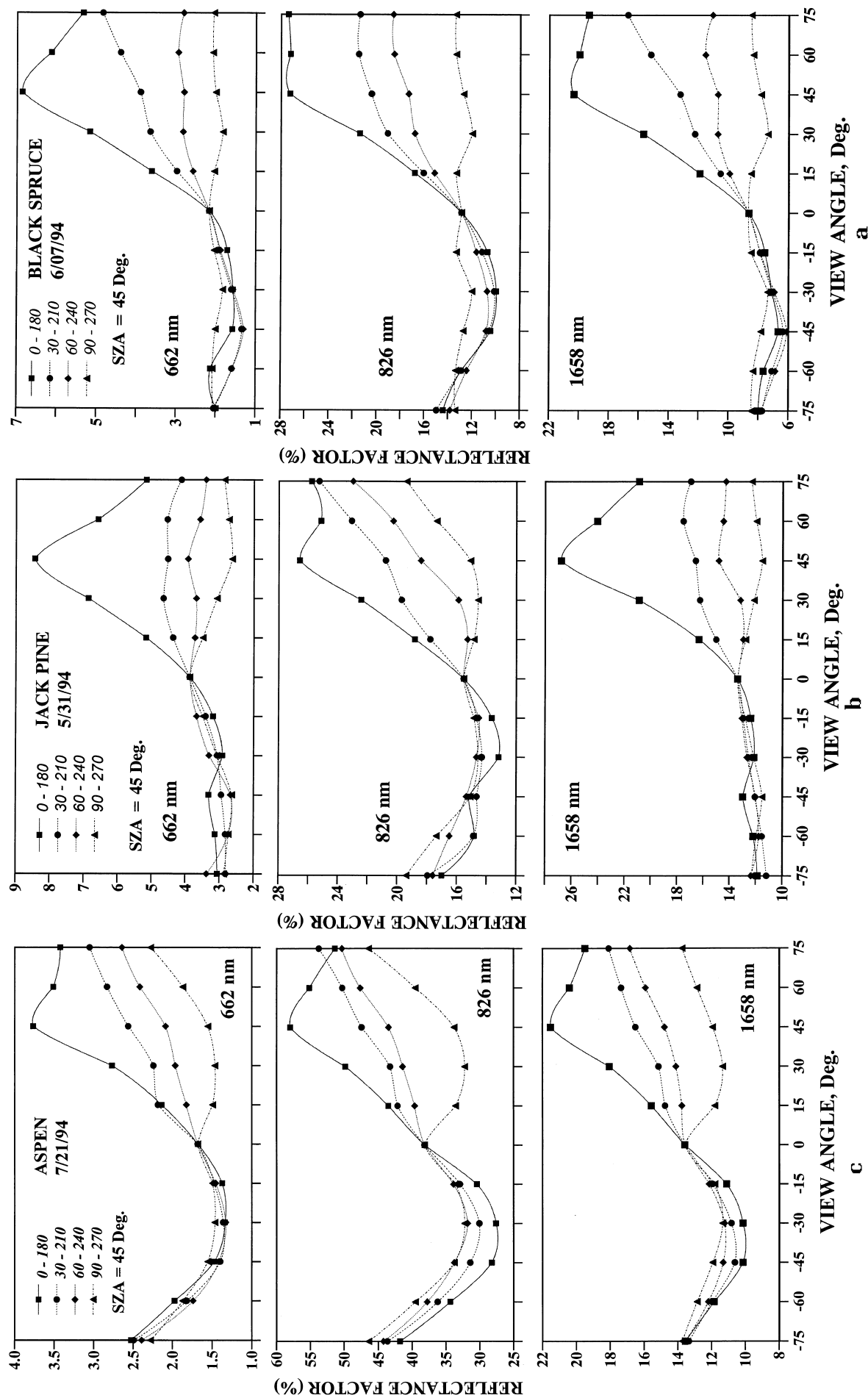


Figure 9. Spectral reflectance factors in four azimuthal transects at 30° azimuthal increments, for three sites, black spruce (a), jack pine (b), and aspen (c), at 45° SZA. The solar principal plane is the 0–180° plane while the plane perpendicular to it is the 90–270° plane.

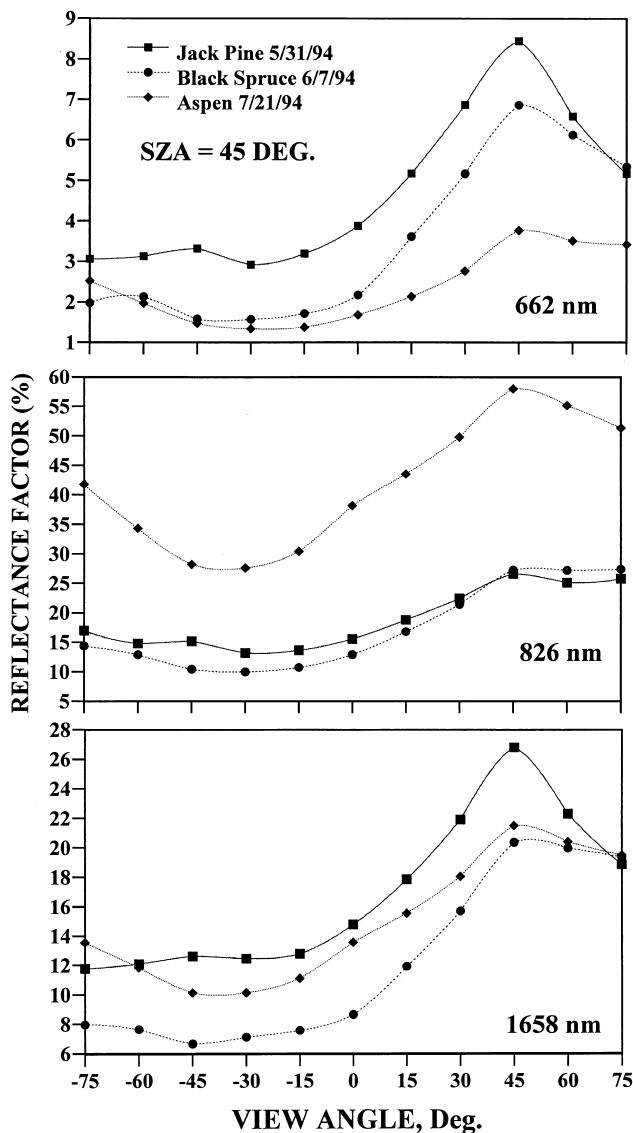


Figure 10. Comparison of the spectral reflectance factor magnitudes for the three sites, in the solar principal plane at 45° SZA.

pal plane. Of course, the differences in canopy density, geometry, understory, and species composition vary considerably between these sites. At the Sweden spruce site there were approximately 680 trees/ha with an average height of 18.5 m, while at the Maine spruce-hemlock site there were approximately 1200 trees/ha with an average height of 14.5 m. However, even with all the differences in species, canopy heights, and understory between these sites, all the spruce sites showed nadir visible reflectances within 1% of each other, although the BOREAS black spruce site showed higher reflectances than the other two sites in the hot spot region. In the NIR waveband, the black spruce and Sweden spruce site reflectances are nearly equal from 60° forwardscatter to 30° backscatter view angles. For the SWIR waveband, the three spruce sites had reflectances which were approximately within 2–5% (absolute) of each other.

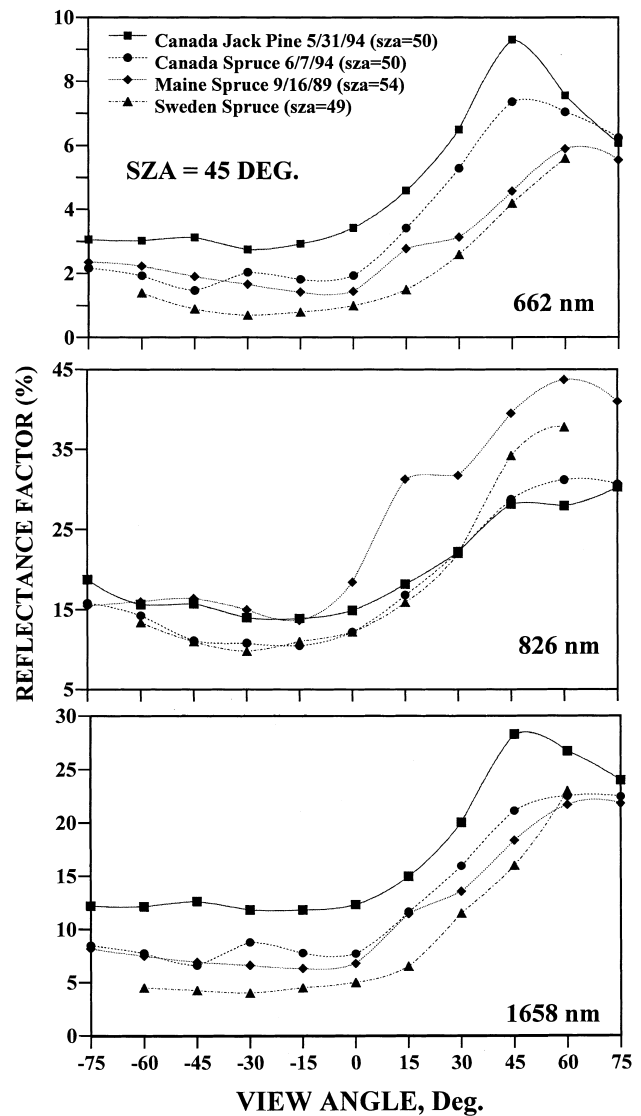


Figure 11. Comparison of the solar principal plane reflectance factors for the coniferous sites, black spruce, and jack pine, with a spruce-hemlock forest in Maine (USA), and a spruce forest in Sweden (Kleman, 1987). The data shown are for a nominal solar zenith angle of 50°, with a range of 49–54° SZA.

Vegetation Indices

Two commonly utilized spectral vegetation indices, the normalized difference vegetation index (NDVI) and the simple ratio (SR), are computed from reflected radiances in the red and NIR wavebands. The NDVI is computed as the difference between the NIR and red radiances divided by the sum $\{NDVI = (NIR - red) / (NIR + red)\}$ and the SR is just the NIR divided by the red radiances $\{SR = NIR / red\}$. In the previous section, these reflected radiances have been shown to be highly anisotropic with differences in anisotropy between the two wavebands, and therefore it would be expected that the vegetation indices would also be anisotropic. These two indices continue to be applied to large scale analysis of the boreal

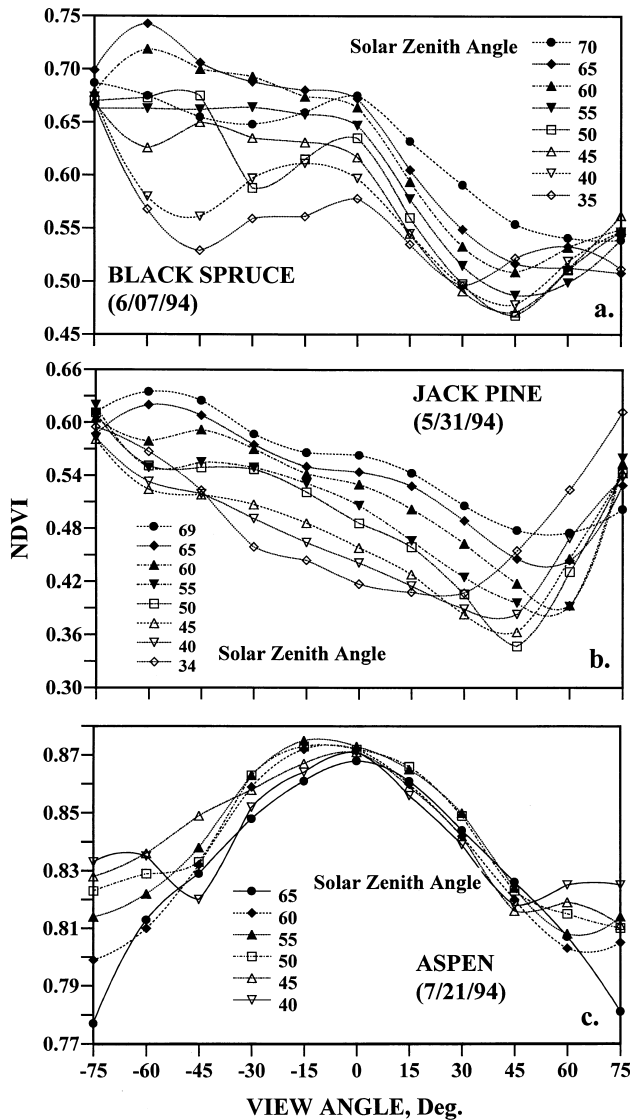


Figure 12. The normalized difference vegetation index (NDVI) as a function of SZA in the solar principal plane for the a) black spruce, b) jack pine, and c) aspen sites.

forest such as Bonan's (1991b) use of NDVI for tree carbon flux estimation and the analysis presented in Sellers et al. (1995) in which the relation between SR and CO₂ flux between the atmosphere and vegetation is analyzed.

The dynamics of the NDVI as a function of SZA and view angle in the solar principal plane are shown in Figure 12. For the jack pine site, the minimum NDVI occurs at the view angle corresponding to the location of the hot spot maximum, due to the larger hot spot effect in the red versus the NIR (see Fig. 6). For all SZAs at the jack pine site, there is a nearly linear increase in NDVI, from the hot spot to -75° forwardscatter, as increasingly more shadowed elements are viewed, and as a result of larger increases in NIR than red reflected radiances. Also noted is the trend at most view angles (with the exception of the hot spot region and very large forwardscatter angles) of increasing NDVI as SZA increases.

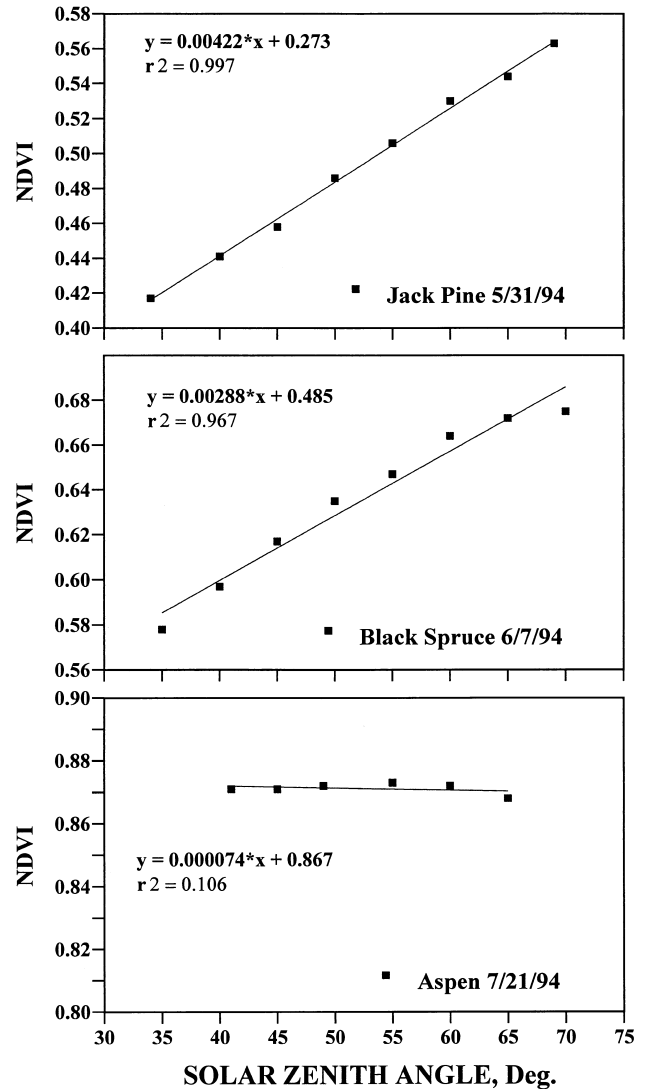


Figure 13. Variation of nadir view NDVI as a function of SZA for all three sites.

This variation with SZA is largest at nadir and is linear as a function of SZA (Fig. 13.) This trend of NDVI in SZA can be attributed to the greater shadowing in the red than the NIR and the significant difference between the red reflectance of sunlit versus shadowed reindeer moss. Sellers (1985) modeled a linear trend in NDVI as a function of SZA for a canopy with LAI of 1.0 and vertical leaf angle distribution. Although the jack pine needles are not all vertically oriented, the tree crown structure of the incomplete canopy presents a somewhat clumped vertical structure. In contrast, Sellers (1985) modeled a nearly constant value of NDVI at nadir, regardless of leaf angle for a canopy with a large LAI=4.0. The NDVI at nadir view for the canopy with the highest LAI which we studied, aspen (LAI=5.5), is also nearly constant as a function of SZA (Fig. 13).

The NDVI of the black spruce site (Fig. 12) also shows hot spot minimums and an increase in the NDVI

from the hot spot to the nadir view direction. However, for the nadir to the -60° forwardscatter view angle direction, the NDVI is relatively constant for the black spruce (as compared to increasing for jack pine), possibly due to the denser crown structure of the black spruce resulting in similar transmittance effects in both wavelengths. The nadir and near-nadir values of NDVI show a nearly linear trend of increasing NDVI as SZA increases (Fig. 13), but with a smaller change in NDVI (0.029 per 10° SZA change) than the jack pine site (0.042 per 10° SZA change), perhaps due to darker background reflectances of mixed shrubs and moss species at this site and therefore less visible reflectance difference between shadowed and sunlit background than for the jack pine site.

The aspen site shows a significantly different view and Sun angle dependence of the NDVI, compared to the coniferous sites, due to the combination of higher LAI, differing canopy geometry, different background composition, and different leaf properties and geometries. In the solar principal plane, this site shows peak NDVI values at nadir which decrease in off-nadir view angle in both the forward scatter and backscatter view directions (Fig. 12). The double layer structure of the canopy, with the lower layer hazelnut canopy actually having higher LAI, explains why the near-nadir views (which see the largest percentage of understory) have higher NDVI than far off-nadir views, which are seeing just the canopy top layer of the aspen trees. As mentioned previously, there is a weaker visible hot-spot effect in the aspen site versus the two coniferous sites, and, since the hot spot magnitude is similar in both the red and NIR for the aspen, there is very little hot spot signature on the NDVI at the aspen site.

The variability in NDVI for other azimuth planes, including the solar principal plane, at 45° SZA is shown in Figure 14. For the jack pine site, as previously noted for spectral reflectances (Fig. 9.), the hot-spot effect is completely avoided at 30° azimuth angle offset from the solar principal plane. Jupp and Strahler (1991) also show this avoidance of hot spot effects in the NDVI for view azimuths that are not in the solar principal plane, for a modeled canopy with LAI=2.9. For all planes except the solar principal plane, there is an increase in NDVI for the jack pine site when viewing at increasing off-nadir view angles in both forward and back view directions, since at nadir the sensor views the highest percentage of background (light-colored lichen), contrasting with viewing the green-needled tree top at far off-nadir view angles.

For the black spruce site, there is also an elimination of the hot spot minimum in NDVI for the azimuth which is 30° from the solar principal plane. However, in contrast to the jack pine, the forward scatter view direction NDVI values are higher than the backscatter. For the plane perpendicular to the solar principal plane the NDVI is nearly constant as a function of view angle.

The aspen site shows a maximum NDVI near-nadir

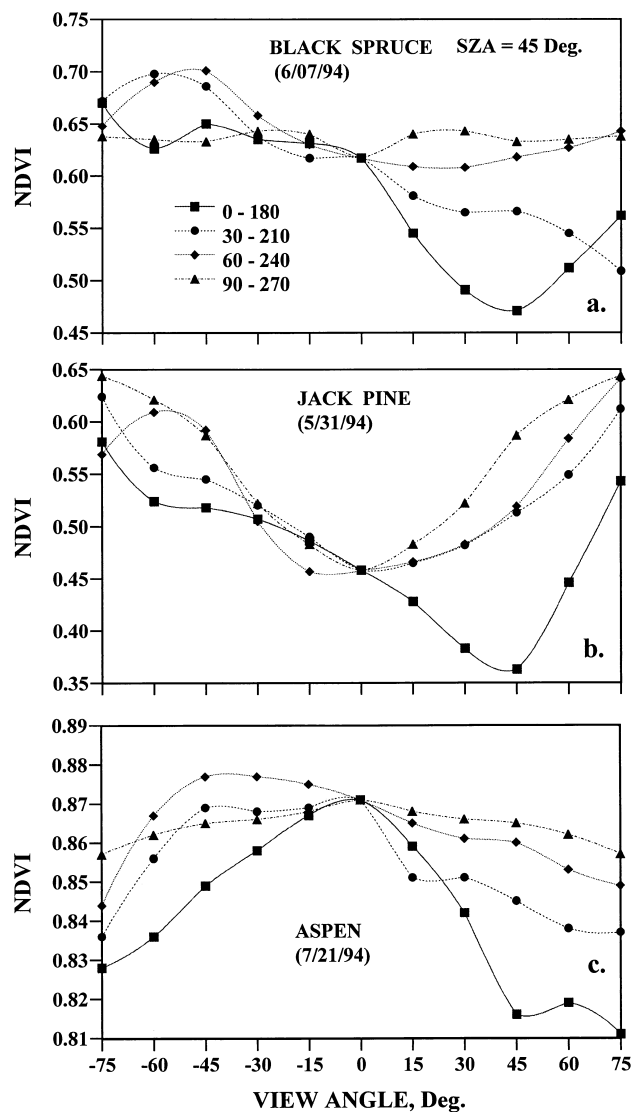


Figure 14. NDVI in four azimuthal transects at 30° azimuthal increments, for three sites, black spruce (a), jack pine (b), and aspen (c) at 45° SZA. See Figure 9 for reflectance factors in these same view angle planes.

to 45° off-nadir in the forward scatter direction for all azimuth planes and less variation in NDVI for view azimuths not in the solar principal plane. The variation in NDVI with view angle is much lower for this site than for the coniferous sites, with the exception of the view azimuth perpendicular to the solar principal plane for the black spruce site.

The variation of the SR with view angle and solar zenith angle in the solar principal plane (Fig. 15) is nearly identical in form to variation of the NDVI. The nadir values of SR for both the black spruce and the jack pine show a linear increase with increasing solar zenith angles. This variation in SR with SZA may explain in part the divergence in SR and CO_2 flux as measured by MacPherson and Desjardins from an aircraft flying a ~ 500

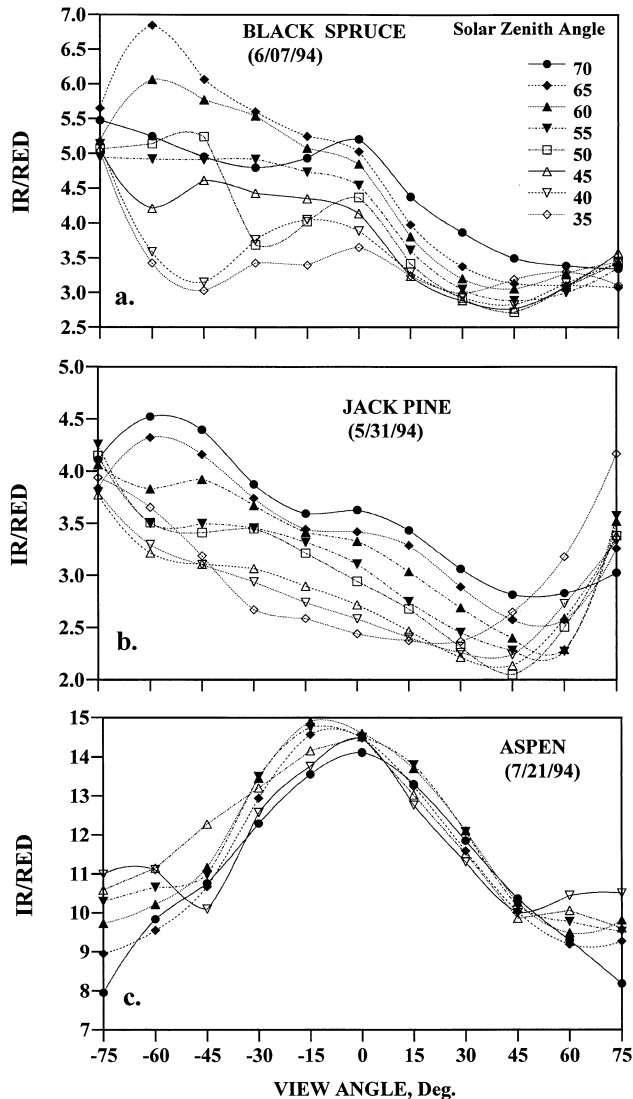


Figure 15. Same as Figure 12, but for the simple ratio (SR) of red/NIR reflected radiances.

km transect from the BOREAS southern study area to the northern study area (Sellers et al., 1995). Normalization of the SR to values near to solar noon SZA would result in a lower SR for the northern half of the transect and thus a closer agreement between SR and CO_2 flux which would be closer to the high correlation shown for the first half of the 250 km transect.

Hemispheric Spectral Reflectances

Hemispheric spectral reflectances have been computed by angular integration of the PARABOLA bidirectional measurements, utilizing data from nadir to 82° view zenith angle in all azimuth planes. Using an analytical function fit (Ahmad and Deering, 1992) to the bidirectional reflectance factor measurements, the reflectance factor values are computed at very small intervals of viewing geometry, which can then be numerically integrated to ob-

tain hemispheric reflectance. The results of these computations are shown in Figures 16a–c as a function of solar zenith angle for the three boreal forest canopies. The spectral hemispheric reflectances for the aspen site increase as solar zenith angle increases from 40° to 65° for all three spectral wavebands. Referring to Figure 6c. of the aspen site bidirectional reflectances in the solar principal plane, it is seen that as the solar zenith angle increases, the reflectances at large off-nadir view angles ($60\text{--}75^\circ$) increase while near-nadir reflectances remain relatively constant. Thus, spectral hemispheric reflectance increasing as SZA increases is due to increased bidirectional reflectance at large view angles, for the aspen site.

At the jack pine site (Fig. 16b) the red hemispheric reflectance shows no coherent trend with SZA, and the SWIR band shows very little trend also, especially if the 69° SZA observation is excluded. However, the near-infrared hemispheric reflectance for the jack pine site does show a very strong increasing trend as SZA increases. Again, referring back to the principal plane bidirectional reflectances for the jack pine site (Fig. 6b), it is noted that, for the near-nadir and hot-spot view angles, the red and SWIR wavebands show higher reflectances at lower solar zenith angles and that this is countered by reflectances generally increasing as SZA increases for 60° and 75° backscatter view angles. Therefore, the net overall effect is a cancelling out of the trends in near-nadir and hot-spot view angles by trends in far off-nadir view angles as a function of SZA. This was not the case for the NIR waveband at the jack pine site, where there was a nearly linear increase of hemispherical reflectance as SZA increased due to strong increases in far off-nadir view angle reflectances as a function of SZA increase, with small changes at the nadir and near-nadir view angles.

The black spruce site hemispherical reflectances show an increase as a function of SZA for all three wavebands. The magnitude of the increase in the red waveband is very small; however, with hemispheric reflectance ranging from only about 2.6% to 3.0% for a SZA range of $35\text{--}70^\circ$. Chen (1996) found that the hemispheric PAR albedo for these same black spruce and jack pine sites was nearly invariant for $\text{SZA} < 70^\circ$, similar to what we have observed for the red waveband (which is a subset of the PAR wavelength interval) at these two sites. Referring back to Figure 6a of the principal plane reflectances of the black spruce site, it is seen that the trends in the visible waveband are similar to those observed for the jack pine, but the magnitude of the hot spot maximum is somewhat lower.

Forest Canopy Total Albedo

The spectral hemispheric reflectances computed from PARABOLA angularly integrated bidirectional reflectance factor measurements were utilized to compute the total albedo ($0.3\text{--}4.0\ \mu\text{m}$) for the aspen site on 21 July 1994

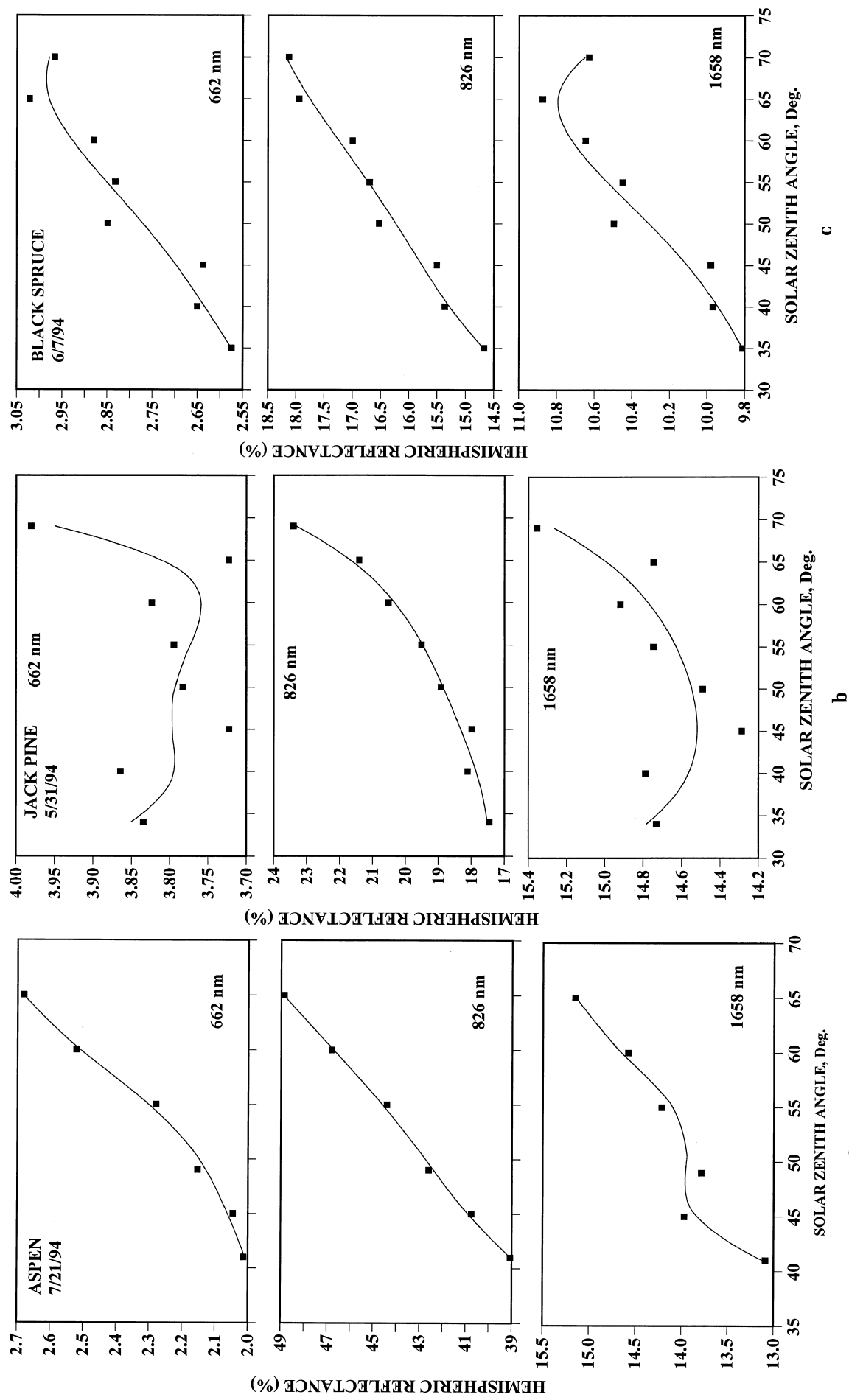


Figure 16. Hemispheric spectral reflectances as a function of solar zenith angle for the a) aspen, b) jack pine, and c) black spruce sites.

and for the jack pine site on 31 May 1994. We were unable to make albedo measurements on the black spruce site on 7 June 1994 due to a damaged pyranometer. The measured total albedos for the aspen and jack pine are shown in Figure 17. Two sets of albedo measurements made at these sites are shown, however, the same instrument type, both upward and downward viewing Eppley PSP pyranometers, were utilized by both investigator teams at the sites. We (the RSS-1 team) made albedo measurements with a downward viewing pyranometer suspended from the same tram system as the PARABOLA instrument was mounted on. We averaged only those measurements for which the tram was deemed to be level, which for these sites and dates were tram positions from 11 m to 7 m from the scaffold tower. The AFM-7 team measurements of albedo were made from pyranometers mounted on a separate smaller tower located approximately 200 m from the main scaffold tower.

Possible reasons for the differences in total albedo measured at the two locations within the study sites are instrument calibration and inhomogeneity of the forest canopy albedo in the study area. Inhomogeneity may be the result of differences in tree density, understory canopy differences, and moisture differences, among other forest stand characteristics. In addition, the presence of huts to house computers, data loggers, and instruments and the location of wooden walkways in the instrument's field of view may have influenced the albedo measurements made by RSS-1. The presence of support towers also had some influence on the albedo measurements made by both groups at both sites. It is noted that the albedos measured by the AFM-7 group are higher than those measured by the RSS-1 group for both the aspen and jack pine sites and that the magnitude of the difference varies by approximately 0.005–0.02, depending on solar zenith angle and site.

We estimate total shortwave albedo (300–4000 nm) using the hemispheric reflectances computed from the three narrow bandwidth PARABOLA channels. Measurements made in these three bands were assumed to represent three broadband spectral regions: 300–700 nm, 700–1300 nm, and 1300–4000 nm. The selection of these specific ranges for the broadband regions was based in part on the variation in spectral reflectance with wavelength of green vegetation and on published measurements which characterize the fraction of total solar energy in the photosynthetically active radiation (PAR) waveband (400–700 nm) and ultraviolet band (300–400 nm). We assumed the amount of total insolation in the 300–700 nm band to be 52% for our calculations, from 700–1300 nm to be 36% and from 1300–4000 nm to be 12% based on the analysis given in Eck et al. (1997). Simulations with the SPCTRAL2 model (Bird and Riordan, 1986) for low aerosol optical depths show that the percentage of irradiance in the 1300–4000 nm waveband is practically constant at 12% over a wide range of solar

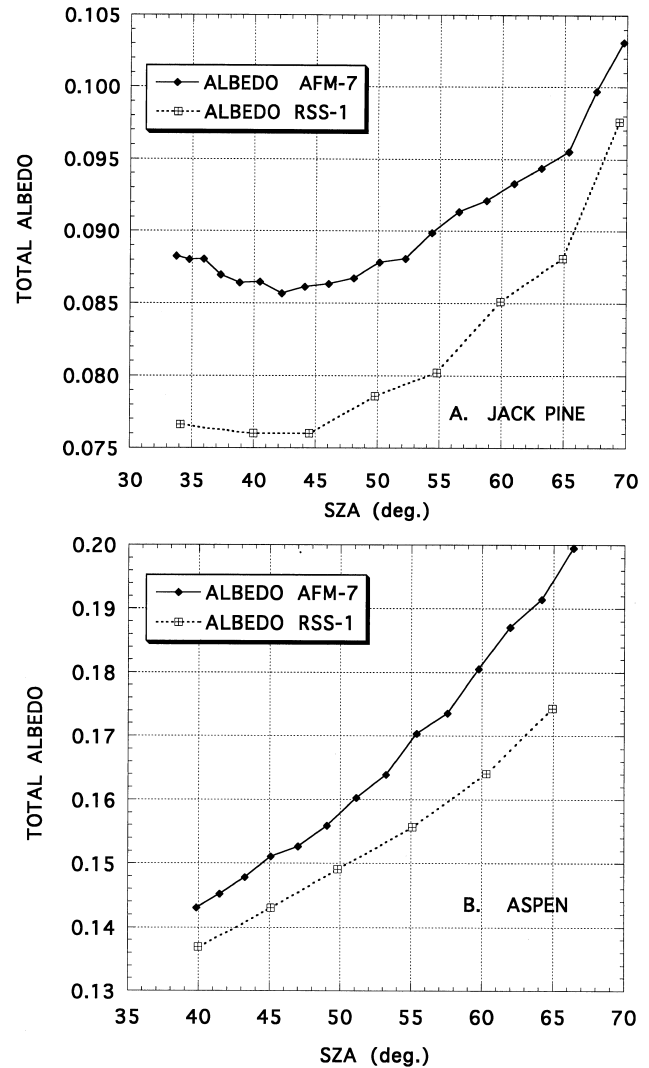


Figure 17. Total albedo measured by upward and downward viewing Eppley PSP pyranometers at a) the jack pine site and b) the aspen site. Albedo measurements were made from two different tower systems located approximately 100–200 m from each other.

zenith angles. In addition, Weiss and Norman (1985) measured PAR fraction to be 0.46 over a wide range of solar zenith angles. Therefore, we hold the relative fractions of irradiance for the three broadband regions as constant values as a function of solar zenith angle. These relative percentages of incident solar radiation are very similar to the values determined independently by Brest and Goward (1987), which were 52.6% for 300–725 nm, 36.2% for 725–1400 nm, and 11.2% for 1400–4000 nm.

Inspection of the vegetation reflectance spectra of any green vegetation suggests that the failure to account for the weighting of the narrowband PARABOLA reflectances to the vegetation reflectance spectra across the broadband spectral regions may have contributed to the errors in the estimates of albedo (Eck et al., 1997). Therefore, we computed reflectance weighting factors

(W_{RFLi}) to account for the reflectance variation in the three broadband regions as

$$W_{RFLi} = \frac{\int_{LBBi}^{UBBi} R(\lambda)E(\lambda) d\lambda / \int_{LBBi}^{UBBi} E(\lambda) d\lambda}{\int_{LPAi}^{UPAi} R(\lambda)E(\lambda) d\lambda / \int_{LPAi}^{UPAi} E(\lambda) d\lambda} \quad (2)$$

where

- $R(\lambda)$ =spectral reflectance as a function of wavelength
- $E(\lambda)$ =spectral incident solar radiation ($W/m^2 \mu m$)
- $UBBi$ =upper wavelength for broadband region (μm)
- $LBBi$ =lower wavelength for broadband region (μm)
- $UPAi$ =upper wavelength for PARABOLA spectral band (μm)
- $LPAi$ =lower wavelength for PARABOLA spectral band (μm)

The data set we used for $R(\lambda)$ was the measured spectral reflectances of alfalfa, at seven biomass and canopy coverage levels (including bare soil) from 450 nm to 2360 nm (Deering, 1989), since there were no measurements available (at the time of this analysis) of high resolution reflectance spectra for the boreal forest canopies over a wide spectral range from ultraviolet to shortwave infrared. These measurements were made with a Barnes 12-550 Spectroradiometer at nadir view angle and a solar zenith angle of 55°. The alfalfa canopy data used in this study were selected to match as closely as possible the NDVI computed from spectral reflectance from the alfalfa measurements to the NDVI computed from PARABOLA measured spectral reflectances at the aspen and jack pine sites, respectively. For future analysis of this data, it may be possible to utilize reflectance spectra for these same boreal forest sites. However, it is noted that for regional or global satellite retrievals of albedo from sensors such as AVHRR, prior knowledge of the spectral reflectance characteristics of the surface are unknown. Therefore, the analysis as we are implementing it here would be more representative of what might be done in the case of satellite remote sensing estimates. Also, reflectance spectra are utilized for relative weighting within each of three broadband regions, and thus the absolute magnitude of the reflectance is not very important as compared to the relative change within each band.

In order to evaluate Eq. (2) over the entire short-wave spectrum (300–4000 nm), we made some assumptions concerning the vegetation reflectance spectra below 450 nm and above 2390 nm. The spectral hemispheric reflectance of alfalfa measured by Coulson and Reynolds (1971) show a nearly constant reflectivity from 320 nm

to 451 nm for a solar zenith angle range of about 32–75°. We therefore assumed a constant reflectance value, $R(\lambda)$, from 300 nm to 450 nm. For wavelengths from 2360 nm to 4000 nm, we used the measured reflectance value at 2360 nm and assumed a constant value with wavelength. Although we have no measurements to confirm the validity of this assumption, this wavelength interval, 2360–4000 nm, contains only about 1.3% of the total energy in the solar spectrum (300–4000 nm). We used the SPCTRAL2 model (Bird and Riordan, 1986) to calculate spectral incident solar radiation from 300 nm to 4000 nm at 122 wavelengths in Eq. (2) for two solar zenith angles for each site, 40° and 65° for aspen and 35° and 70° for jack pine. These values represented the range of solar zenith angles for which the PARABOLA measurements were taken.

The values of the reflectance weighting factors, W_{RFLi} , computed from Eq. (2), as estimated for the jack pine site and averaged for the two solar zenith angles, were 1.02 for the 300–700 nm band, 0.92 for the 700–1300 nm band, and 0.82 for the 1300–4000 nm band. For the aspen site the estimated values of W_{RFLi} averaged for the two solar zenith angles were 1.22 (300–700 nm), 0.91 (700–1300 nm), and 0.80 (1300–4000 nm). For both sites the differences in the reflectance weighting factors for the two solar zenith angles (35° and 70°) was very small, ranging from 0% to 1.6%. An estimate of the total albedo, A_E , was then computed accounting for the narrow to broadband reflectance weighting from Eq. (3):

$$A_E = \sum A_{Si} W_{IRi} W_{RFLi} \quad (3)$$

where

- i =wavelength region (1=300–700 nm, 2=700–1300 nm, 3=1300–4000 nm),
- A_{Si} =spectral hemispheric reflectance in three PARABOLA wavebands,
- W_{IRi} =percentage of incident total solar radiation in each broadband region (irradiance weighting factor),
- W_{RFLi} =reflectance weighting factor [Eq. (2)] for each broad-band region.

Comparisons of the combined solar irradiance and spectral reflectance weighted estimates of total albedo to the measured albedos are shown in Figure 18. The estimated versus measured albedo from RSS-1 pyranometers show a nearly constant bias of 0.0177 ranging over the narrow range of 0.0160–0.0192 for both the aspen and jack pine sites combined. Thus there is very little random error [root mean squared error (rmse) is 0.0176 for both sites], but the bias is significant, with equal bias in both sites. Instrumental calibration uncertainty alone does not easily explain a constant bias since calibration error should be manifested as a percentage error, not a constant offset. However, since both sites (aspen and jack pine) contain a similar amount of noncanopy struc-

tures, such as huts and wooden boardwalks and metal scaffold towers, it is possible that the bias may result in part from the contamination of the measured albedo by these noncanopy structures. The spectral hemispherical reflectances from PARABOLA data should not have these noncanopy elements contaminating the measurement since statistical outliers are filtered and values of directionally reflected radiances in 15° FOV affected by the tower are excluded by known viewing angle geometry. Comparison of the estimated albedo to albedo measured by the AFM-7 group, however, shows a much smaller bias in the estimates, averaging 0.0083 for the jack pine and 0.0055 for the aspen, with rmse errors of 0.0091 for jack pine and 0.0071 for aspen.. This smaller bias may be partly the result of fewer noncanopy structures contaminating the field of view of the downward viewing pyranometer deployed by the AFM-7 group and may also be due in part to pyranometer calibration. In addition, the limited spectral sampling provided by the PARABOLA instrument and the assumptions made in spectral integration are also sources of uncertainty in estimated albedo and may also have contributed to the observed bias.

It is noted that the bias is not as constant as was the case for the comparison with the RSS-1 pyranometer. This may be partly due to spatial variance in canopy structure between the sites leading to differences in the solar zenith angle dependence of the albedo, as shown in Figure 17. In addition, another possible source of error in albedo measurements may be the cosine response errors of the Eppley PSP pyranometers (Michalsky et al., 1995). These errors increase as the angle of incidence increases, and could be expected to yield underestimates of albedo since the upwelling flux is diffuse with a large percentage of the contribution from large incidence angles versus the dominantly point source downwelling flux (irradiance) resulting from the very low aerosol optical depths.

SUMMARY AND CONCLUSIONS

The spectral bidirectional reflectances of three dominant boreal forest canopy types have been measured under cloudless skies at the phenological growth stages which were at or near to the maximum leaf area index of each site. These measurements were taken under low aerosol optical depth conditions which are characteristic for the southern boreal forest region of central Saskatchewan, when smoke from forest fires is not present. Reflectance factors at the three measured spectral bands with central wavelengths of 662 nm, 826 nm, and 1658 nm showed strong anisotropy at all sites and all wavelengths. Peak backscatter reflectances were observed, with hot spot maxima seen for the black spruce and jack pine sites, while the aspen site showed a much less prominent hot spot peak. Viewing only 30° azimuth angle off from the

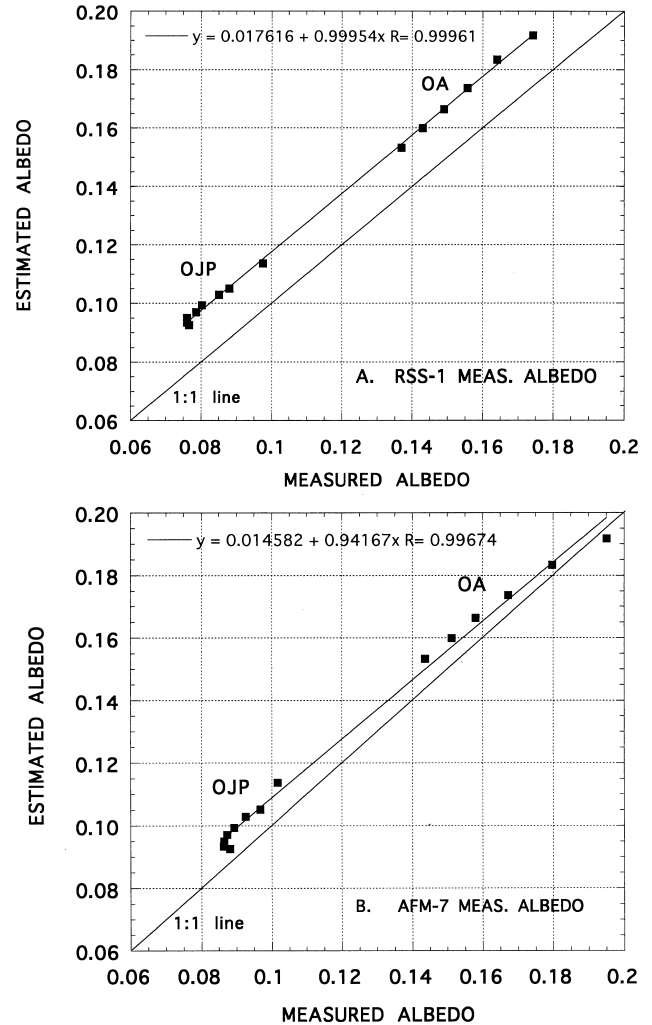


Figure 18. Comparison of total albedo estimated from PARABOLA hemispheric reflectances to pyranometer measured albedos for the aspen (OA) and jack pine (OJP) sites. Albedo estimates are compared to the two different sets of pyranometer albedo measurements made at the two sites shown in Figure 17.

solar principal plane results in a nearly complete avoidance of the hot spot peak. The effects of shadowing within the canopy varied considerably for the three forest canopies studied, due to differences in canopy LAI, geometry, and canopy background or understory characteristics. For near-nadir view directions, the visible reflectances at the jack pine and black spruce sites decreased significantly as solar zenith increased compared to relatively small changes at the aspen site. This results from the large LAI of the understory canopy of hazelnut shrubs at the aspen site contrasted to the light-colored lichen and very low LAI of the understory at the jack pine site.

In contrast to the visible, the near-infrared wavelength reflectance varied very little as a function of SZA at the jack pine site, thus resulting in a large change in

NDVI as a function of SZA. The jack pine site showed a nearly linear increase in nadir view NDVI of 0.042 per 10° SZA change, the black spruce canopy also exhibited a nearly linear trend of 0.029 per 10° SZA, while the aspen nadir NDVI was nearly constant as a function of SZA. These solar zenith angle effects on vegetation indices may be significant in seasonal analyses and need to be taken into consideration when utilizing these indices for remote sensing studies of the boreal region.

The bidirectional reflectances were angularly integrated over the complete upwelling hemisphere to compute spectral hemispheric reflectances. For the black spruce and jack pine sites, the visible hemispheric reflectances showed little and no solar zenith angle dependence, respectively. This is a result of compensating increases in backscatter reflectances as solar zenith angle increases which in part offset the decreases in nadir and near-nadir reflectance as SZA increases. The spectral hemispheric reflectances in the three narrow PARABOLA instrument bandpasses were utilized to estimate the total shortwave albedo of the forest canopies. These spectral hemispheric reflectances were weighted by both spectral irradiance and reflectance to obtain estimates, and these were compared to albedo as measured by pyranometers. The estimated albedos were all biased high but only by approximately 0.018 or 0.007 depending on which set of pyranometer measurements were used in the comparison. Possible reasons for measured albedo differences include instrument calibrations, site "contamination" by structures and support towers, and canopy structure/density differences at the two nearby measurement sites.

The bidirectional reflectance measurement sets reported in this study in conjunction with numerous detailed *in situ* and remotely sensed canopy biophysical properties measured by other BOREAS researchers at these same sites provide a useful data set for the development of forest canopy reflectance models. These models can be utilized in turn to infer biophysical parameters from remotely sensed measurements made over the vast circumpolar boreal zone. In addition to the PARABOLA measurements reported here for the spring–summer phenological growth stage, measurements were also made with the PARABOLA instrument in three other seasons, including winter with snow background. A description and analysis of the seasonal variation in bidirectional reflectances for these three boreal forest sites is the topic of a future article.

PARABOLA data acquisitions and analysis were supported under NASA RTOP 462-61-13 by the Terrestrial Ecology Program of NASA Headquarters managed by Dr. Diane Wickland. The authors thank Piers Sellers and Forrest Hall for their encouragement and support of data acquisitions at the tower/tram sites in BOREAS. The assistance provided in Prince Albert National Park, Saskatchewan by Mary Dahlman, Paula Pacholek, and Tom Hertzog is greatly appreciated. The authors gratefully

acknowledge the development of the PARABOLA data processing and analysis software by Suriaya Ahmad and her adaptation of that software specifically for BOREAS data sets. We also thank the three anonymous reviewers for their constructive criticisms which helped improve this manuscript.

REFERENCES

- Ahmad, S. P. and Deering, D. W. (1992), A simple analytical function for bidirectional reflectance. *J. Geophys. Res.* 97: 18867–18886.
- Bird, R. E., and Riordan, C. (1986), Simple solar spectral model for direct and diffuse irradiance on horizontal and tilted planes at the Earth's surface for cloudless atmospheres. *J. Clim. Appl. Meteorol.* 25:87–97.
- Bonan, G. B. (1991a), Atmosphere-biosphere exchange of carbon dioxide in boreal forests, *J. Geophys. Res.* 96:7301–7312.
- Bonan, G. B. (1991b), Seasonal and annual carbon fluxes in a boreal forest landscape. *J. Geophys. Res.* 96:17,329–17,338.
- Bonan, G. B. (1993), Importance of leaf area index and forest type when estimating photosynthesis in boreal forests. *Remote Sens. Environ.* 43:303–314.
- Breon, F.-M., Vanderbilt, V., Leroy, M., Bicheron, P., Walthall, C. L., and Kalshoven, J. E. (1997), Evidence of a hot spot directional signature from airborne POLDER measurements. *IEEE Trans. Geosci. Remote Sens.* 35:479–484.
- Brest, C. L., and Goward, S. N. (1987), Deriving surface albedo measurements from narrow band satellite data. *Int. J. Remote Sens.* 8:351–367.
- Chen, J. M. (1996), Canopy architecture and remote sensing of the fraction of photosynthetically active radiation absorbed by boreal conifer forests. *IEEE Trans. Geosci. Remote Sens.* 34:1353–1368.
- Chen, J. M., and Cihlar, J. (1996), Retrieving leaf area index of boreal conifer forests using Landsat TM images. *Remote Sens. Environ.* 55:153–162.
- Chen, J. M., Rich, P. M., Gower, T. S., Norman, J. M., and Plummer, S. (1997a), Leaf area index of boreal forests: theory, techniques and measurements. *J. Geophys. Res.* 102: 29,429–29,443.
- Chen, J. M., Blanken, P. D., Black, T. A., Guilbeault, M., and Chen, S. (1997b), Radiation regime and canopy architecture in a boreal aspen forest. *Agric. For. Meteorol.* 86:107–125.
- Coulson, K. L., and Reynolds, D. W. (1971), The spectral reflectance of natural surfaces. *J. Appl. Meteorol.* 10:1285–1295.
- D'Arrigo, R., Jacoby, G. C., and Fung, I. Y. (1987), Boreal forests and atmosphere-biosphere exchange of carbon dioxide. *Nature* 329:321–323.
- Deering, D. W. (1989), Field measurements of bidirectional reflectance. In *Theory and Applications of Optical Remote Sensing* (G. Asrar, Ed.), Wiley, New York, pp. 14–65.
- Deering, D. W., and Leone, P. (1986), A sphere scanning radiometer for rapid directional measurements of sky and ground radiance. *Remote Sens. Environ.* 19:1–24.
- Deering, D. W., Eck, T. F., and Grier, T. (1992), Shinnery oak bidirectional reflectance properties and canopy model inversion. *IEEE Trans. Geosci. Remote Sens.* GE-30(2):339–348.
- Deering, D. W., Middleton, E. M., and Eck, T. F. (1994), Reflectance anisotropy for a spruce-hemlock forest canopy. *Remote Sens. Environ.* 47:242–260.

- Eck, T. F., Deering, D. W., and Vierling, L. A. (1997), Arctic tundra albedo and its estimation from spectral hemispheric reflectance. *Int. J. Remote Sens.* 18:3535–3549.
- Hapke, B., DiMucci, D., Nelson, R., and Smythe, W. (1996), The cause of the hot spot in vegetation canopies and soils: shadow-hiding versus coherent backscatter. *Remote Sens. Environ.* 58:63–68.
- Hunt, E. R., and Rock, B. N. (1989), Detection of changes in leaf water content using near- and middle-infrared reflectances. *Remote Sens. Environ.* 30:43–54.
- Jackson, R. D., Moran, M. S., Slater, P. N., and Bigger, S. F. (1987), Field calibration of reference reflectance panels. *Remote Sens. Environ.* 17:37–53.
- Jacoby, G. C., and D'Arrigo, R. (1995), Tree ring width and density evidence of climatic and potential forest change in Alaska. *Global Biogeochem. Cycles* 9:227–234.
- Jupp, D. L. B., and Strahler, A. H. (1991), A hotspot model for leaf canopies. *Remote Sens. Environ.* 38:193–210.
- Kimes, D. S., Newcomb, W. W., Nelson, R. F., and Schutt, J. B. (1986), Directional reflectance distribution of a hardwood and pine forest canopy. *IEEE Trans. Geosci. Remote Sens.* GE-24:281–293.
- Kleman, J. (1987), Directional reflectance factor distribution for two forest canopies. *Remote Sens. Environ.* 23:83–96.
- Kriebel, K. T. (1978), Measured spectral bidirectional reflectance properties for four vegetated surfaces, *Appl. Opt.* 17: 253–259.
- Kuusk, A. (1991), The angular distribution of reflectance and vegetation indices in barley and clover canopies. *Remote Sens. Environ.* 37:143–151.
- London, J., Bojkov, R. D., Oltmans, S., and Kelley, J. I. (1976), Atlas of the global distribution of total ozone July 1957–June 1967, NCAR Tech. Note 113+STR, Boulder, CO, 276 pp.
- Markham, B. L., Schafer, J. S., Holben, B. N., and Halthore, R. N. (1997), Atmospheric aerosol and water vapor characteristics over north central Canada during BOREAS. *J. Geophys. Res.* 102 (BOREAS Special Issue):29,737–29,745.
- Michalsky, J. J., Harrison, L. C., and Berkheiser, W. E., III (1995), Cosine response characteristics of some radiometric and photometric sensors. *Solar Energy* 54:397–402.
- Nakajima, T., Glauco, T., Rao, R., Boi, P., Kaufman, Y. J., and Holben, B. N. (1996), Use of sky brightness measurements from ground for remote sensing of particulate polydispersions. *Appl. Opt.* 35:2672–2686.
- Ranson, K. J., Daughtry, C. S. T., and Biehl, L. L. (1986), Sun angle, view angle, and background effects on spectral response of simulated balsam fir canopies. *Photogramm. Eng. Remote Sens.* 52:649–658.
- Ranson, K. J., Irons, J. R., and Williams, D. L. (1994), Multi-spectral bidirectional reflectance of northern forest canopies with the Advanced Solid-state Array Spectroradiometer (ASAS). *Remote Sens. Environ.* 47:276–289.
- Schlesinger, M. E., and Mitchell, J. B. F. (1987), Climate model calculations of the equilibrium climatic response to increased carbon dioxide. *Rev. Geophys.* 25:760–798.
- Sellers, P. J. (1985), Canopy reflectance, photosynthesis, and transpiration. *Int. J. Remote Sens.* 6:1335–1372.
- Sellers, P. J., Hall, F. G., Baldocchi, D., et al. (1994), The BOREAS experiment plan, Version 3.0, NASA BOREAS Report, Goddard Space Flight Center, Greenbelt, MD.
- Sellers, P., Hall, F., Margolis, H., et al. (1995), The Boreal Ecosystem-Atmosphere Study (BOREAS): an overview and early results from the 1994 field year. *Bull. Amer. Meteorol. Soc.* 76:1549–1577.
- Spanner, M. A., Pierce, L. L., Peterson, D. L., and Running, S. W. (1990), Remote sensing temperate coniferous forest leaf area index. The influence of canopy closure, understory, and background reflectance. *Int. J. Remote Sens.* 11:95–111.
- Vermote, E., Tanré, D., Deuze, J. L., Herman, M., and Morcrette, J. J. (1997), Second simulation of the satellite signal in the solar spectrum, 6S: an overview. *IEEE Trans. Geosci. Remote Sens.* 35:675–686.
- Verstraete, M. M., Pinty, B., and Myneni, R. B. (1996), Potential and limitations of information extraction on the terrestrial biosphere from satellite remote sensing. *Remote Sens. Environ.* 58:201–214.
- Waggoner, A. P., Weiss, R. E., Ahlquist, N. C., Covert, D. S., Will, S., and Charlson, R. J. (1981), Optical characteristics of atmospheric aerosols. *Atmos. Environ.* 15:1891–1909.
- Weiss, A., and Norman, J. M. (1985), Partitioning solar radiation into direct and diffuse, visible and near infrared components. *Agric. For. Meteorol.* 34:205–213.